J Biomol NMR (2015) 63:417–423
DOI 10.1007/s10858-015-9996-6

NMR STRUCTURE NOTE

Structures of the reduced and oxidized state of the mutant D24A of yeast thioredoxin 1: insights into the mechanism for the closing of the water cavity

Anwar Iqbal[1,2] · Adolfo Henrique Moraes[1,2] · Ana Paula Valente[1,2] · Fabio C. L. Almeida[1,2]

Received: 18 July 2015 / Accepted: 14 October 2015 / Published online: 20 October 2015

Biological context or introduction

Thioredoxins (Trx) are ubiquitous proteins that are present in all living organisms. All Trxs share a typical characteristic fold and contain the conserved catalytic motif Trp–Cys–Pro–Gly–Cys (Holmgren 1979; Kallis and Holmgren 1980). Trxs display disulfide reductase activity and interact with multiple cellular targets. Trxs show a conserved fold, which is composed of a central hydrophobic β-sheet (β_1, β_2, β_3, β_4 and β_5) surrounded by four α-helices (α_1, α_2, α_3 and α_4). The interacting loops are the catalytic loop (β_2, α_2), β_3–α_3 loop, α_3–β_4 loop and β_5–α_4 loop (Pinheiro et al. 2008b; Bao et al. 2009a). Figure 1a shows the typical fold of yTrx, the active site loops and the important residues facing the water cavity.

An essential structural element is the conserved and ancestral water cavity. We recently demonstrated that the water cavity has the catalytic relevant events of coupling hydration, motions of the interacting loops and H^+ exchange (Cruzeiro-Silva et al. 2014; Iqbal et al. 2015). It is comprised between α-helix 2 and 4, the central β-sheet and underneath the interacting loops (Fig. 1a). The key residues facing the water cavity are the conserved Asp24, Lys54 and *cis*-Pro73. The water cavity is caged by the presence of the three conserved proline residues: Pro32, *cis*-Pro 73, and Pro38, maybe to strengthen the formation of cavity by accomplishing a relative rigidity and hydrophilicity as structural requirements (Iqbal et al. 2015).

An internal tightly bound water at the cavity near the buried aspartic acid is a conserved feature present in all species studied so far (Bao et al. 2009b; Weichsel et al. 2010; Campos-Acevedo et al. 2013). The crystal structure of yeast Trx1 (yTrx1) determined for the oxidized form showed a tightly bound water molecule near the Asp24 (Bao et al. 2009a). There is a queue of water molecules entering into the cavity along Ile36 and staying close across the Asp24, with only one internal water molecule, which is bridging Asp24 and Cys33. This water molecule is involved in catalytic activity by mediating the proton transfer from the buried cysteine to the buried aspartate (Cys33 to Asp24 for yTrx1) (Langsetmo et al. 1991; LeMaster et al. 1997; Menchise et al. 2001).

Our group recently showed that in solution the water cavity is expanded, when compared to the crystal structure of yTrx1. There is in average five internal water molecules in continuous exchange with the bulk water (Cruzeiro-Silva et al. 2014). Molecular dynamics (MD) simulation validated by nuclear relaxation data shows that the cavity is formed by three contiguous lobes (Iqbal et al. 2015). Lobe A and C are exposed to the protein surface and responsible for the water exchange while lobe B is central, containing the catalytic residues Cys33 and Asp24. There is a strong correlation between protein dynamics at multiple time-scales and the water cavity. All residues showing conformational exchange are next to or indirectly in contact with the water cavity.

Electronic supplementary material The online version of this article (doi:10.1007/s10858-015-9996-6) contains supplementary material, which is available to authorized users.

✉ Fabio C. L. Almeida
falmeida@cnrmn.bioqmed.ufrj.br

[1] Institute of Medical Biochemistry, National Center of Nuclear Magnetic Resonance Jiri Jonas, Federal University of Rio de Janeiro, Av. Carlos Chagas Filho, 373 CCS/Anexo CNRMN, Rio de Janeiro, RJ 21941-920, Brazil

[2] Center of Structural Biology and Bioimaging (CENABIO), Federal University of Rio de Janeiro, Rio de Janeiro, Brazil

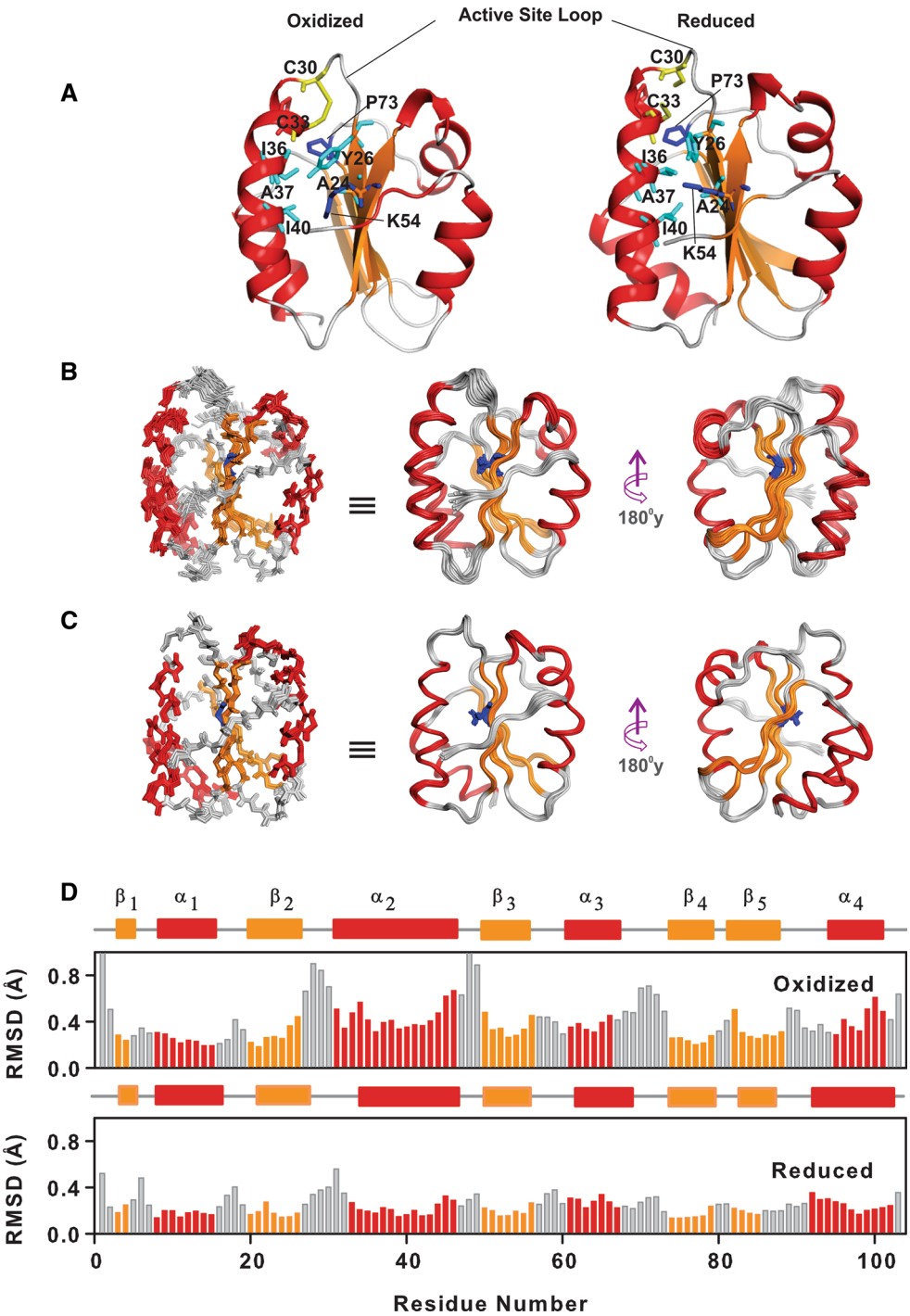

Fig. 1 Trx structure ensembles of oxidized and reduced state of D24A mutant: **a** ribbon representation of the oxidized (*left*) and reduced (*right*) D24A mutant of yTrx1. The structure shows the active site loop, containing both exposed Cys30 and the buried Cys33 (*yellow*). It also shows the important residues that are facing the water cavity: Pro73, Lys54 (*blue*) and Ala24, Tyr26, Ile36, Ala37 and Ile40 (*cyan*). **b**, **c** Representation of the ensemble of the 20 lowest-energy structures of oxidized (**b**) and reduced (**c**) D24A yTrx1. Wire representation of the backbone is in the *left* and the ribbon representation in the *right* in two orientations. **d** Backbone atoms root mean square deviation (RMSD) from de mean structure as a function of residue number for D24A yTrx1 oxidized (*top*) and reduced (*bottom*). The graph is *color-coded* according the secondary structure elements: *red* for the α-helices, *orange* for β-strands and *grey* for loops

The mutation of Asp24 also alters the protein dynamics. The mutation D24A caused the quenching of the dynamics of the residues facing the central lobe B (Iqbal et al. 2015). The closing of the central lobe for this mutant is further supported by the measurement of mutational frustration (Jenik et al. 2012; Iqbal et al. 2015). Residues involved in dynamics are frequently highly frustrated. The mutation D24A reduce considerably the mutational frustration levels (Iqbal et al. 2015).

The presence of the conserved Asp24 tightly bound to a water molecule supports the model that explain the activation of Cys33, which ultimately leads to the breakage of the mixed disulfide between Trx and the target protein. The model assumes that the water molecule bridges Cys33 thiol to Asp24, facilitating the proton transfer that increase the nucleophilicity of Cys33 (stabilization of Cys33 thiolate) (Cruzeiro-Silva et al. 2014). In the current work, we present the structure of the mutant D24A in the oxidized and

reduced state. The structures helped the understanding of the integrity of water cavity and of the positioning of the catalytic relevant residues and their functional groups orientation in hydrophobic core. The side chain of the conserved residues such as Tyr26 changed their orientation closing the central lobe of the water cavity.

Methods and results

The *E. coli* strain BL21(DE3) have been transformed with the pET3a vector containing the gene coding for *Saccharomyces cerevisiae* Trx1 (yTrx1) D24A mutant. In minimal medium (M9), uniform ^{15}N and ^{13}C isotope labeling were assured by providing ^{15}N labeled NH_4Cl and $^{13}C_6$ D-glucose (Cambridge Isotope, USA) in the growth medium as the sole source for nitrogen and carbon, respectively. Cells were allowed to grow to OD_{600} of 0.7 at 37 °C, shaking at 80 RPM and then added of 1 mM final concentration of isopropyl β-D-1-thiogalactopyranoside (IPTG, Sigma-Aldrich, USA) for induction of protein expression for 3 h at 37 °C. After harvesting the cells by centrifugation for 30 min at 6000*g*, the cells were suspended in lysis buffer containing 50 mM of Tris:HCl pH 8.0, phenylmethanesulfonylfluoride (PMSF) and 10 mM of dithiothreitol (DTT) and disrupted by sonication. The cells debris were spin down at 8000*g*, for 30 min at 4 °C. The supernatant were purified by Q-Sepharose column (GE Lifescience, USA), using the buffer combination of solution A (20 mM Tris–HCl pH 8.0, 10 mM DTT) for loading protein sample followed by ionic gradient of buffer B (20 mM Tris–HCl pH 8.0, 10 mM DTT, 1 M, NaCl). After dialysis against 20 mM phosphate buffer to remove the excess of DTT, four times excess of diamide (Sigma-Aldrich, USA) were used for oxidation of cysteines for 30 min followed by size exclusion Sephacryl 26/60 resin (GE Lifescience, USA) for further purification. The purity of protein were confirmed by 15 % SDS polyacrylamide gel electrophoresis (SDS-PAGE).

NMR spectroscopy

The NMR spectra were collected on a Bruker Avance III 600-MHz spectrometer with a cryogenic probe head. The double-labeled ($^{15}N/^{13}C$) D24A mutant was prepared at a concentration of 850 µM in 20 mM phosphate buffer pH 7.0 in H_2O/D_2O (10 %) for oxidized and reduced yTrx1 D24A mutant. The protein backbone resonance assignments were achieved through analysis of the triple resonance experiments: HNCACB, CBCA(CO)NH, and HNCO (Ikura et al. 1990; Wittekind and Mueller 1993). The aliphatic side-chain resonances were primarily assigned using HBHA(CO)NH (Grzesiek and Bax 1993) experiment and with the help of complementary HCCH-TOCSY (Kay et al. 1993), HCCH COSY (Bax et al. 1990), ^{15}N-edited NOESY-HSQC and ^{13}C-edited NOESY-HSQC (Sattler 1999) optimized for both aliphatic or aromatic region detection. Assignments of aromatic side chains were obtained using NOEs between the aromatic protons and the $^{\beta}CH_2$ group in the ^{13}C-NOESY-HSQC spectrum. The data were processed using NMRpipe (Delaglio et al. 1995) or TopSpin3.1 (Bruker Biospin) while resonance assignments were achieved using the software CCPNMR Analysis (Vranken et al. 2005).

Structure calculation

Structure calculation of the D24A mutant (both oxidized and reduced state) were performed iteratively using ARIA program, version 2.2 (Linge et al. 2001; Rieping et al. 2007) combined with CNS version 1.2 (Brunger et al. 1998). We used CCPNMR Analysis interface with Aria2.1 (Rieping et al. 2007). NOE-based distance constraints used in the structure calculation were extracted from, ^{15}N NOESY-HSQC and ^{13}C-NOESY-HSQC datasets. The angle restraints of phi and psi of the protein backbone dihedral angles were predicted based on analysis of ^{1}HN, ^{15}N, $^{1}H\alpha$, $^{13}C\alpha$, ^{13}CO, and $^{13}C\beta$ chemical shifts using the program TALOS N (Shen et al. 2009; Shen and Bax 2013).

The structures were calculated with CNS 1.2 using torsion angle simulated annealing protocol. Several cycles of ARIA were performed using standard protocols. After each cycle rejected restraints, side-chain assignments, NOEs and dihedral violations were analyzed. Finally, 400 conformers were calculated with ARIA/CNS, and among them, the 20 best water-refined structures with the lowest energy were selected to represent the solution structural ensemble of yTrx1 D24A.

The structures ensembles were visualized and analyzed with MOLMOL (Koradi et al. 1996) and Pymol (DeLano 2002) while their quality validation were assessed using PROCHECK (Laskowski et al. 1996) and Common Interface for NMR structure Generation (CING) for data validation (Doreleijers et al. 2012).

Structure determination of yTrx1 D24A mutant

D24A in the oxidized and reduced state is monomeric in solution and present the typical Trx folding. The ^{15}N–^{1}H HSQC spectra of D24A displayed sharp and dispersed peaks indicating that the protein is well structured. The ^{1}H, ^{15}N, and ^{13}C resonances of D24A mutant (oxidized and reduced) at pH 7.0 20 mM phosphate buffer and 25 °C

Table 1 List of restraints and statistical analysis for reduced and oxidized state of D24A mutant

	Reduced state	Oxidized state
Number of experimental restraints		
Total NOE distance restrains	1304	1272
Intraresidue	422	503
Sequential	253	261
Short range ($2 \leq \|I - j\| \leq 3$)	253	111
Medium range ($4 \leq \|I - j\| \leq 5$)	42	60
Long range ($\|I - j\| > 5$)	209	197
Torsion angle (phi/psi)	176	170
H-bond restraints	54	56
RMSD from average structure (Å) *for the reduced state*		
Backbone (3-4,8-15,20-26,33-46,51-56,61-67,74-79,82-85,92-102)	0.3	
Backbone, all atoms	0.2	
Heavy atoms (3-4,8-15,20-26,33-46,51-56,61-67,74-79,82-85,92-102)	0.8	
Heavy atoms, all residues	0.8	
RMSD from average structure (Å) *for the oxidized state*		
Backbone (3-5,8-15,20-26,31-46,50-56,61-66,74-79,82-88,95-101)		0.4
Backbone, all atoms		0.4
Heavy atoms (3–5,8–15,20–26,31–46,50–56,61–66,74–79,82–88,95–101)		0.9
Heavy atoms, all residues		0.9
Restraints violations		
NOE violations (> 0.5 Å)	1	1
Dihedral angle (> 5°)	0	1
Deviations from ideal Geometry[a]		
RMS for bond lengths (Å)	0.006 ± 0.0002	0.0060 ± 0.0002
RMS for bond angles (°)	0.8 ± 0.016	0.9 ± 0.017
Ramachandran plot of ordered residues (%)[b]		
Most favored regions	86.4 %	87.2 %
Allowed regions	13.4 %	11.6 %
Generously allowed	0.3 %	1.1 %
Disallowed	0.0 %	0.1 %
Energy (kcal mol^{-1})		
E_{Totol}	−3938 ± 63.28	−3520.2 ± 79.1
E_{Bond}	32.98 ± 2.5	41.84 ± 2.8
E_{Angle}	159 ± 7.8	189 ± 10.8
E_{Vdm}	−1001.6 ± 5.8	−965 ± 9.9
E_{Elec}	−4008.08 ± 61.7	−3716 ± 62
E_{Impar}	343.88 ± 25.64	386.30 ± 57

[a] Deviation from ideal geometry and Energy[c] were calculated using CNS Solve protocols. [b] The RMSD calculation and PROCHECK analyses were performed for the ensemble of the 20 lowest energy structures using PSVS suite

have been assigned (95 % oxidized and 96 % reduced) and deposited in the BMRB under accession number 25702 (reduced D24A Mutant) and 25703 (oxidized D24A Mutant). The NMR restraints and coordinates of 20 best structures of the yeast yTrx1 mutant D24A in the reduced and oxidized state has been deposited in Protein Data Bank under code number 2N5A and 2N5B respectively.

Figure 1 shows the ensemble of oxidized (B) and reduced (C) conformer of D24A and their superimposition of backbone of an ensemble of 20 lowest energy structures, revealing a good agreement with NMR restraints. A summary of structural statistics for the 20 lowest energy conformers is in Table 1. The root mean square deviations (RMSDs) from the average structure of these structures

Table 2 Pairwise Cα root mean square deviation (RMSD) of the D24A mutant and wild type yTrx1 (WT) in both reduced and oxidized states

RMSD (Å)	D24A reduced	D24A oxidized	WT reduced	WT oxidized
D24A reduced	–	1.33	1.66	1.10
D24A oxidized		–	1.74	0.780
WT reduced			–	1.35
WT oxidized				–

The RMSD was calculated using the software Pymol (DeLano 2002), which takes into consideration only secondary structure elements. The PDB structures 3F3Q (Bao et al. 2009a) and 2I9H (Pinheiro et al. 2007) were used to calculate the RMSD

were 0.4 ± 0.12 Å and 0.9 ± 0.20 Å (oxidized) and 0.3 ± 0.12 Å and 0.8 ± 0.18 Å (reduced) for the backbone and heavy atoms, respectively. The Ramachandran analysis for reduced D24A indicated a good geometry, with 100 % of residues in allowed regions of the Ramachandran and 86 % in the most favored region. The structure of the D24A in the oxidized state also show good geometry with 99.9 % of the residues in allowed regions of the Ramachandran, with 87.2 % residues in the most favored region.

Overview of the D24A: the conformational and biological importance

The presence of the conserved proton acceptor (Asp24 for yTrx1) near the buried cysteine is a recognized important feature of Trxs. The activity of disulfide reduction toward insulin decreases 10–15 times upon mutation of buried Asp to Ala (Dyson et al. 1997; Iqbal et al. 2015). We recently showed that the mutant D24A of yTrx1 closes the central lobe B of the water cavity, decreasing consistently the water access to the cavity. The water cavity remains opened through lobes A and C (Iqbal et al. 2015).

Table 2 shows the root mean square deviation (RMSD) between the structures of mutant D24A and wild type yTrx1. The overall structural change elicited by the mutation D24A was more pronounced for the reduced state than for the oxidized state. We found an RMSD of 0.780 Å for the comparison of the oxidized D24A and wild type yTrx1 and 1.66 Å for the reduced states. The difference between the oxidized and reduced states were very similar for the D24A (1.33 Å, Table 2) and the wild type yTrx1 (1.35 Å, Table 2) (Pinheiro et al. 2008a; Bao et al. 2009a). The introduction of mutation induced local and non-local changes. The changes dissipated thorough the protein mainly by hydrophobic core residues.

Several residues, such as Tyr26, Cys33, Ile36, Ala37, Ile40, Glu41, Val88 for the reduced state and Tyr26, Cys33, Ile36, Ala37, Ile40, Phe52, and Lys54 for the oxidized state, reorient and surround the water cavity in an entirely different fashion. In the oxidized state, Tyr26, Ile36 and Ile40 side chains rearrangement induced the splitting of the cavity in two portions (Lobes A and C, Fig. 2a, b). The same happened for the reduced state (Fig. 2c, d). Tyr26 is essential, since it fill the space left by the substitution of Asp24 by Ala24. This local effect is a consequence of global hydrophobic rearrangement. This effect has been observed before by MD simulation (Iqbal et al. 2015). While MD simulation gives a description of this effect with discrete structure, the solution structure shows that in average we observed the same property described by the MD simulation and validated by NMR relaxation experiments.

We also compared the NMR structures with the MD simulations, which based the description of the cavity for both oxidized and reduced states. Figure S1 shows the pairwise RMSD obtained for the NMR ensembles and compared with an ensemble of 100 structure randomly extracted from the 200 ns MD simulations. For both the oxidized and reduced states, the NMR ensemble is contained in the MD ensemble, resulting in RMSDs significantly smaller for the NMR ensembles. The MD ensemble showed an expanded conformational space, resulting in higher values of RMSDs for both the oxidized and reduced states. We also compared the MD ensemble with and ensemble that combined the MD and NMR ensembles. We did not observed a significant increase in RMSD for the combined MD//NMR ensembles. It means that the NMR ensemble is within the conformational space of the MD ensemble. There are few exceptions, such as the loop β5-α4 for both the oxidized and reduced states. We also looked at the orientation of the key side chains that are facing the water cavity. In all cases, the side chain orientation of the NMR ensemble is contained in the MD ensemble. The only exception is Val88, which is located in the loop β5-α4.

Besides the lack of a proton acceptor, the closing of lobe B of the cavity might be the main reason for the severe decrease of the activity (< 10 times) for the mutant D24A residue by changing the hydration equilibrium of the protein. In summary, the D24A structural determination

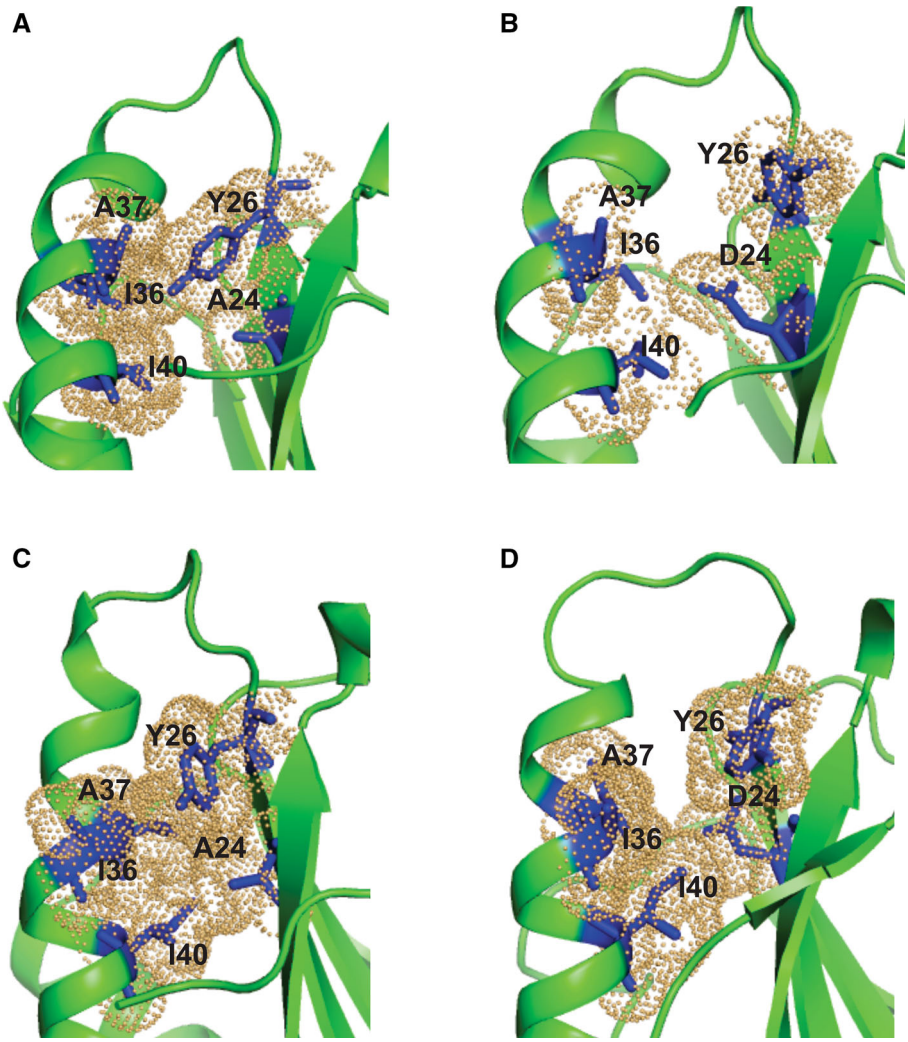

Fig. 2 Comparison of the core residues of the D24A and wild type yTrx1 in oxidized and reduced states: the structure as *zoomed* in the region that contains the water cavity and the active site. The representation of the side chains of the selected residues, Ala/Asp24, Y26, Ile36, Ala37 and Ile40 are shown in *blue sticks* **a** and **c** represents D24A mutant in oxidized state and reduced state, respectively. **b** and **d** represents wild type yTrx1 in oxidized state and reduced states, respectively. We used 2I9H and 3F3Q as the wild type yTrx1 structures. The residues highlighted in *blue* are the same shown in *cyan* in Fig. 1a

confirms the structural variation at the hydrophobic core of the protein leading to the dissection of the water cavity. Furthermore, the mutation of D24A was not enough to close fully the hydrophobic cavity: lobes A and C remains.

In summary, the present work provided structural information to understand the properties of the hydrophobic rearrangement experimented by yTrx1 upon changes in the water cavity. The conformational information induced by changes in internal hydration is passed along by a global rearrangement of the hydrophobic core. The global structural changes leaded to the partial closing of the water cavity, at the central lobe B.

Acknowledgments We are thankful to the financial support from CNPq, FAPERJ and INBEB for supporting this work (Brazilian funding agencies). We are also thankful to the National Center of Nuclear Magnetic Resonance (CNRMN) for the NMR time.

Compliance with ethical standards

Conflict of interest The authors declare no conflict of interest.

References

Bao R, Zhang Y, Lou X et al (2009a) Structural and kinetic analysis of Saccharomyces cerevisiae thioredoxin Trx1: implications for the catalytic mechanism of GSSG reduced by the thioredoxin system. Biochim Biophys Acta 1794:1218–1223. doi:10.1016/j.bbapap.2009.04.001

Bao R, Zhang Y, Zhou C-Z, Chen Y (2009b) Structural and mechanistic analyses of yeast mitochondrial thioredoxin Trx3 reveal putative function of its additional cysteine residues. Biochim Biophys Acta 1794:716–721. doi:10.1016/j.bbapap.2008.12.016

Bax A, Clore GM, Driscoll PC et al (1990) Practical aspects of proton–carbon–carbon–proton three-dimensional correlation

spectroscopy of 13C-labeled proteins. J Magn Reson 87:620–627. doi:10.1016/0022-2364(90)90320-9

Brunger AT, Adams PD, Clore GM et al (1998) Crystallography & NMR system: a new software suite for macromolecular structure determination. Acta Crystallogr Sect D Biol Crystallogr 54:905–921

Campos-Acevedo AA, Garcia-Orozco KD, Sotelo-Mundo RR, Rudiño-Piñera E (2013) Expression, purification, crystallization and X-ray crystallographic studies of different redox states of the active site of thioredoxin 1 from the whiteleg shrimp *Litopenaeus vannamei*. Acta Crystallogr Sect F Struct Biol Cryst Commun 69:488–493. doi:10.1107/S1744309113010622

Cruzeiro-Silva C, Gomes-Neto F, Machado LESF et al (2014) Hydration and conformational equilibrium in yeast thioredoxin 1: implication for H+ exchange. Biochemistry 53:2890–2902. doi:10.1021/bi401542v

Delaglio F, Grzesiek S, Vuister GW et al (1995) Nmrpipe—a multidimensional spectral processing system based on UNIX pipes. J Biomol NMR 6:277–293

DeLano WL (2002) The PyMol molecular graphics system, version 1.7.4.4. Schrodinger, LLC

Doreleijers JF, Sousa da Silva AW, Krieger E et al (2012) CING: an integrated residue-based structure validation program suite. J Biomol NMR 54:267–283. doi:10.1007/s10858-012-9669-7

Dyson HJ, Jeng MF, Tennant LL et al (1997) Effects of buried charged groups on cysteine thiol ionization and reactivity in *Escherichia coli* thioredoxin: structural and functional characterization of mutants of Asp 26 and Lys 57. Biochemistry 36:2622–2636. doi:10.1021/bi961801a

Grzesiek S, Bax A (1993) Amino acid type determination in the sequential assignment procedure of uniformly 13C/15N-enriched proteins. J Biomol NMR 3:185–204. doi:10.1007/BF00178261

Holmgren A (1979) Reduction of disulfides by thioredoxin. Exceptional reactivity of insulin and suggested functions of thioredoxin in mechanism of hormone action. J Biol Chem 254:9113–9119

Ikura M, Kay LE, Bax A (1990) A novel approach for sequential assignment of proton, carbon-13, and nitrogen-15 spectra of larger proteins: heteronuclear triple-resonance three-dimensional NMR spectroscopy. Application to calmodulin. Biochemistry 29:4659–4667. doi:10.1021/bi00471a022

Iqbal A, Gomes-Neto F, Miyamoto CA et al (2015) Dissection of the water cavity of yeast thioredoxin 1: the effect of a hydrophobic residue in the cavity. Biochemistry 54:2429–2442. doi:10.1021/acs.biochem.5b00082

Jenik M, Parra RG, Radusky LG et al (2012) Protein frustratometer: a tool to localize energetic frustration in protein molecules. Nucleic Acids Res 40:348–351. doi:10.1093/nar/gks447

Kallis GB, Holmgren A (1980) Differential reactivity of the functional sulfhydryl groups of cysteine-32 and cysteine-35 present in the reduced form of thioredoxin from *Escherichia coli*. J Biol Chem 255:10261–10265

Kay LE, Xu GY, Singer AU et al (1993) A gradient-enhanced HCCH-TOCSY experiment for recording side-chain 1H and 13C correlations in H2O samples of proteins. J Magn Reson Ser B 101:333–337. doi:10.1006/jmrb.1993.1053

Koradi R, Billeter M, Wuthrich K (1996) MOLMOL: a program for display and analysis of macromolecular structures. J Mol Graph 14:51–55

Langsetmo K, Fuchs J, Woodward C (1991) The conserved, buried aspartic acid in oxidized *Escherichia coli* thioredoxin has a pKa of 7.5. Its titration produces a related shift in global stability. Biochemistry 30:7603–7609

Laskowski RA, Rullmann JAC, MacArthur MW et al (1996) AQUA and PROCHECK-NMR: programs for checking the quality of protein structures solved by NMR. J Biomol NMR 8:477–486

LeMaster DM, Springer PA, Unkefer CJ (1997) The role of the buried aspartate of Escherichia coli thioredoxin in the activation of the mixed disulfide intermediate. J Biol Chem 272:29998–30001

Linge JP, O'Donoghue SI, Nilges M (2001) Automated assignment of ambiguous nuclear overhauser effects with ARIA. Methods Enzymol 339:71–90

Menchise V, Corbier C, Didierjean C et al (2001) Crystal structure of the wild-type and D30A mutant thioredoxin h of *Chlamydomonas reinhardtii* and implications for the catalytic mechanism. Biochem J 359:65–75

Pinheiro AS, Amorim GC, Eduardo L et al (2007) NMR solution structure of the reduced form of thioredoxin 1 from *Saccharomyces cerevisiae*. Proteins 70:584–587. doi:10.1002/prot

Pinheiro AS, Amorim GC, Netto LES et al (2008a) NMR solution structure of the reduced form of thioredoxin 1 from *Saccharomyces cerevisiae*. Proteins Struct Funct Bioinform 70:584–587

Pinheiro AS, Amorim GC, Netto LES et al (2008b) NMR solution structure of the reduced form of thioredoxin 1 from *Saccharomyces cerevisiae*. Proteins 70:584–587. doi:10.1002/prot.21693

Rieping W, Habeck M, Bardiaux B et al (2007) ARIA2: automated NOE assignment and data integration in NMR structure calculation. Bioinformatics 23:381–382. doi:10.1093/bioinformatics/btl589

Sattler M (1999) Heteronuclear multidimensional NMR experiments for the structure determination of proteins in solution employing pulsed field gradients. Prog Nucl Magn Reson Spectrosc 34:93–158. doi:10.1016/S0079-6565(98)00025-9

Shen Y, Bax A (2013) Protein backbone and sidechain torsion angles predicted from NMR chemical shifts using artificial neural networks. J Biomol NMR 56:227–241. doi:10.1007/s10858-013-9741-y

Shen Y, Delaglio F, Cornilescu G, Bax A (2009) TALOS+: a hybrid method for predicting protein backbone torsion angles from NMR chemical shifts. J Biomol NMR 44:213–223. doi:10.1007/s10858-009-9333-z

Vranken WF, Boucher W, Stevens TJ et al (2005) The CCPN data model for NMR spectroscopy: development of a software pipeline. Proteins 59:687–696. doi:10.1002/prot.20449

Weichsel A, Kem M, Montfort WR (2010) Crystal structure of human thioredoxin revealing an unraveled helix and exposed S-nitrosation site. Protein Sci 19:1801–1806. doi:10.1002/pro.455

Wittekind M, Mueller L (1993) HNCACB, a high-sensitivity 3D NMR experiment to correlate amide-proton and nitrogen resonances with the alpha- and beta-carbon resonances in proteins. J Magn Reson Ser B 101:201–205. doi:10.1006/jmrb.1993.1033